

A novel zerovalent manganese for removal of copper ions: synthesis, characterization and adsorption studies

A. O. Dada¹ · F. A. Adekola² · E. O. Odebunmi³

Received: 25 December 2014 / Accepted: 26 October 2015 / Published online: 20 November 2015
© The Author(s) 2015. This article is published with open access at Springerlink.com

Abstract Synthesis of nanoscale zerovalent manganese (nZVMn) by chemical reduction was carried out in a single pot system under inert environment. nZVMn was characterized using a combination of analytical techniques: Ultraviolet–Visible Spectroscopy, Fourier Transform Infrared Spectroscopy, Scanning Electron Microscopy, Transmission Electron Microscopy, Energy Dispersive X-ray, BET surface area and Point of Zero Charge. The adsorption physicochemical factors: pH, contact time, adsorbent dose, agitation speed, initial copper ion concentration and temperature were optimized. The kinetic data fitted better to Pseudo second-order, Elovich, fractional power and intraparticle diffusion models and their validity was tested by three statistical models: sum of square error, Chi-square (χ^2) and normalized standard deviation (Δq). Seven of the two-parameter isotherm models [Freundlich, Langmuir, Temkin, Dubinin–Kaganer–Raduskevich (DKR), Halsey, Harkin–Jura and Flory–Huggins] were used to analyse the equilibrium adsorption data. The Langmuir monolayer adsorption capacity ($Q_{\max} = 181.818$ mg/g) obtained is greater than other those of nano-adsorbents utilized in adsorption of copper ions. The equilibrium

adsorption data were better described by Langmuir, Freundlich, Temkin, DKR and Halsey isotherm models considering their coefficient of regression ($R^2 > 0.90$). The values of the thermodynamic parameters: standard enthalpy change ΔH° (+50.27848 kJ mol⁻¹), standard entropy change ΔS° (203.5724 J mol⁻¹ K⁻¹) and the Gibbs free energy change ΔG° revealed that the adsorption process was feasible, spontaneous, and endothermic in nature. The performance of this novel nanoscale zerovalent manganese (nZVMn) suggested that it has a great potential for effective removal of copper ions from aqueous solution.

Keywords Manganese nanoparticles · Copper · Characterization · Kinetics · Isotherm · Thermodynamics

List of symbols

C_0	Initial concentration of the Cu ²⁺ solution (mg L ⁻¹)
C_e	Equilibrium concentration of the Cu ²⁺ (mg L ⁻¹)
W	Dry weight in gram of the nZVMn nano-adsorbent
V	Volume of the Cu ²⁺ solution (L)
Q_e	Amount of Cu ²⁺ adsorbed at equilibrium per unit weight of nZVMn (mg g ⁻¹)
q_t	Amount of Cu ²⁺ adsorbed at any time (mg/g)
k_1	Pseudo first-order rate constant (min ⁻¹)
k_2	Pseudo second-order adsorption rate constant (g/mg min)
h_1	Pseudo first-order initial adsorption rate (mg/g min)
h_2	Pseudo second-order initial adsorption rate (mg ² /g ² min)

✉ A. O. Dada
dada.oluwasogo@lmu.edu.ng

✉ F. A. Adekola
fadekola@unilorin.edu.ng

¹ Department of Physical Sciences, Industrial Chemistry, Landmark University, P.M.B.1001, Omu-Aran, Kwara, Nigeria

² Department of Industrial Chemistry, University of Ilorin, P.M.B. 1515, Ilorin, Nigeria

³ Department of Chemistry, University of Ilorin, P.M.B. 1515, Ilorin, Nigeria

α	Constant in the Elovich rate equation (g min ² /mg)
β	Constant in the Elovich rate equation (g min/mg)
k	Fractional power rate constant
R	Gas constant (J/mol K)
K_F	Freundlich isotherm constant
n_F	Exponent in Freundlich isotherm
Q_{\max}	Langmuir maximum monolayer coverage capacity of nZVMn (mg g ⁻¹)
K_L	Langmuir isotherm constant (L mg ⁻¹)
R_L	Dimensionless constant referred to as separation factor
b_T	Temkin isotherm constant related to the heat of adsorption
A_T	Temkin isotherm equilibrium binding constant (Lg ⁻¹)
A_{DKR}	DKR isotherm constant (mol ² /kJ ²) related to free adsorption energy
Q_d	The theoretical isotherm saturation capacity (mg/g)
ε	Polanyi potential = $RT \ln(1 + 1/C_e)$
E	Mean adsorption free energy
K_H and n_H	Halsey constants
A_{HJ} and B_{HJ}	Harkin–Jura constants
θ	Degree of surface coverage
n_{FH}	Flory–Huggins' number of metal ions occupying adsorption sites
K_{FH}	Flory–Huggin's equilibrium constant
k_{id}	Intraparticle diffusion rate constant (mg g ⁻¹ min ^{0.5})
C	Thickness of the boundary
R^2	Regression coefficient
SSE	Sum of square error
χ^2	Chi-square test
Δq	Normalized standard deviation (%)
ΔH°	Standard enthalpy change (J mol ⁻¹)
ΔS°	Standard entropy change (J mol ⁻¹ K ⁻¹)
ΔG°	Standard Gibbs free energy (J mol ⁻¹)
T	Absolute temperature (K)
K_c	Thermodynamic equilibrium constant

Introduction

Nanotechnology is the science of structuring matters into a large surface area which holistically possesses unique characteristics. This is part of modern science and its applications attract interest of researchers owing to the fact that it gives room for several innovations. The application of nanotechnology to waste water remediation vis-à-vis

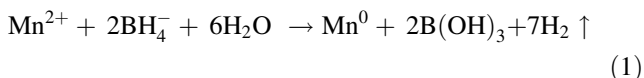
heavy metal ions removal cannot be over emphasized (Dada et al. 2014a, b). The effectiveness of nanomaterials is majorly enhanced by its surface area (Jain et al. 2007; Prathna 2012). Copper is often released into the environment through anthropogenic activities. Soluble copper compounds post a number of threats to human health. Usually, water-soluble copper compounds occur in the environment through applications in agriculture. Copper toxicity affects human beings, aquatic organisms and plants (Roosta et al. 2014; Wojtysiak and Kudelski 2012). A number of adverse effects of copper exist due to over-exposure ranging from irritation of the nose, mouth and eyes, headaches, stomachaches, dizziness, vomiting, hematemesis, diarrhoea, hypotension, melena, coma, jaundice to liver and kidney damage and even death (Bonnie et al. 2007; Brewer 2010). However, several methods such as precipitation, cementation, reverse osmosis, ion-exchange, electro-dialysis have been used to remove these heavy metals; yet, the problems still persist because of myriad of limitations of these methods (Prasad and Elumalai 2011). Adsorption has proven to be an efficient and cost-effective method of combating this problematic and toxic heavy metal ion. Some researchers have reported the use of some nano-adsorbents such as amino-functionalized magnetic nanoparticles (Kumar and Yadav 2011), pectin–iron oxide magnetic nanocomposite (Xi et al. 2011) for the adsorption of copper(II) ions. Nevertheless, to the best of our knowledge, there has been no report on preparation, characterization and adsorption studies of copper onto nanoscale zerovalent manganese (nZVMn). There are no data on detailed kinetic and isotherm models of adsorption of Cu(II) onto nanoscale manganese. Therefore, the objectives of this study are: to investigate the synthesis of nanoscale zerovalent manganese (nZVMn) in a single pot system using bottom-up approach via chemical reduction; carrying out the characterization of nZVMn and investigate its application in adsorption of Cu(II) ions. The effect of adsorbent dose, stirring speed, contact time, pH, initial Cu(II) concentration and temperature was investigated. The kinetic data were tested with pseudo first-order, pseudo second-order, Elovich, Fractional Power (Power function), and intraparticle diffusion models to determine the rate of adsorption and mechanism of the process. The equilibrium data were also subjected to seven isotherm models: Langmuir, Freundlich, Temkin, Dubinin–Kaganer–Raduskevich (DKR), Halsey and Harkin–Jura and Flory–Huggins. The thermodynamic parameters such as enthalpy change (ΔH), entropy change (ΔS) and Gibb's free energy change (ΔG) were calculated. The post adsorption characterization of the adsorbent (nZVMn) was carried out using scanning electron microscope (SEM) and energy dispersive X-ray (EDX). Finally, the effect of salinity on adsorption of Cu(II) onto nZVMn was determined.

Materials and methods

Materials and synthesis

All the reagents used are of analytical grade. Deionized deoxygenated water (sparged with nitrogen gas) was used all through for this synthesis. Sodium borohydride (Sigma-Aldrich, USA) was used for the chemical reduction, other reagents used were: $\text{MnCl}_2 \cdot 4\text{H}_2\text{O}$ (Xilong Chemical, China), Absolute Ethanol (BDH) and HNO_3 (Sigma-Aldrich, USA).

Nanoscale zerovalent manganese was synthesized by chemical reduction method in a single pot system via bottom-up approach (Dada et al. 2014a, b; Boparai et al. 2010; Chen et al. 2011; Liu (2008); Edison and Sethuraman 2013). In a typical procedure for nanoscale zerovalent manganese synthesis, 0.023 M of $\text{MnCl}_2 \cdot 4\text{H}_2\text{O}$ was prepared and tagged solution A and 0.123 M NaBH_4 was prepared and tagged solution B. Manganese chloride was reduced to zerovalent manganese according to the reaction below:



Under inert condition in a glove box, solution B was added in drops to solution A in a three-neck round-bottom flask and rapid formation of zerovalent manganese with faint brownish colour was observed with a large evolution of hydrogen gas. As soon as the borohydride solution was added to manganese chloride solution, a faint brownish nanoparticle (nZVMn) appeared and the mixture was further stirred for 3 h. Excess of borohydride solution was needed for better formation of nZVMn. However, nanoscale zerovalent manganese (nZVMn) was allowed to age overnight. nZVMn was separated from the solution using vacuum filtration apparatus and a cellulose nitrate membrane filter (Millipore filter) of 0.45 μm . The nZVMn was further washed with absolute ethanol three times and dried in a Genlab oven at 50 °C overnight to obtain a deep brown colour of nZVMn.

Characterization of nZVMn

The adsorption band arising from the surface plasmon resonance in the nZVMn was determined using a Beckmann Coulter DU 730 Life Science UV–VIS spectrophotometer.

The information on the molecular environment of nZVMn was obtained from the spectrum recorded using Shimadzu FTIR model IR 8400S.

The surface morphology and elemental composition were determined using scanning electron microscopy (SEM) integrated with energy dispersive X-ray (EDX)

analyzer. SEM images and EDX spectra were obtained using a TESCAN Vega TS 5136LM typically at 20 kV at a working distance of 20 mm. Samples for SEM analysis were prepared by coating them in gold using a Balzers' Sputtering device.

The transmission electron microscopy (TEM) was carried out using A Zeiss Libra 120 transmission electron microscope at 80 kV voltage. This was useful to determine the size and shape of the nanostructure.

The determination of surface area, pore size and volume was done using Brunauer–Emmett–Teller (BET) and Barrett, Joyner, Halenda (BJH) methods.

The pH Point of Zero charge (pH pzc) is the pH at which the nZVMn surface submerged in an electrolyte (0.1 M NaNO_3) exhibits zero net charge. This was carried out using the procedure reported by Srivastava et al. 2005. The pH was varied from 2 to 12 by adjustments with 0.1 M HNO_3 or 0.1 M NaOH .

Adsorption experiment

Batch adsorption studies

Batch adsorption experiment was done by contacting 100 mg of the nZVMn in 60 mL of Teflon bottle with 50 mL of Cu^{2+} concentrations intermittently for 3 h at optimum operational conditions. The mixture was filtered and the filtrate was immediately analysed for Cu^{2+} ions concentrations using atomic adsorption spectrophotometer (AAS) model AA320 N. The determination of the residual concentration using AAS was done in triplicate and the mean value for each set of the experiments was calculated. Investigation of other operational parameters such as effects of pH, contact time, adsorbent dose, temperature and ionic strength was carried out following a similar procedure (Adekola et al. 2012; Hao et al. 2010). Adsorption capacity and the removal efficiency were obtained using Eqs. 2 and 3, respectively (Hameed et al. 2008):

$$Q_e = \frac{(C_o - C_e)V}{W}, \quad (2)$$

$$\%RE = \frac{C_o - C_e}{C_o} \times 100, \quad (3)$$

where Q_e is the equilibrium adsorption capacity per gram dry weight of nZVMn (mg g^{-1}), V is the volume of the Cu^{2+} solution (L), C_o is the initial concentration of the adsorbate solution before adsorption (mg L^{-1}), C_e is the equilibrium concentration of the Cu^{2+} after adsorption (mg L^{-1}), W is the dry weight in gram of the nZVMn nano-adsorbent. The adsorption kinetics was conducted at optimum operational parameters as stated at the bottom of

the plot from 10 to 120 min. The kinetic data were fitted to five kinetic and mechanism models: pseudo first-order, pseudo second-order, Elovich, Fractional Power (Power function), and intraparticle diffusion models.

Effect of initial concentration was investigated by varying initial concentrations from 10 to 200 ppm at optimum conditions. The equilibrium data were fitted to seven isotherm models: Langmuir, Freundlich, Temkin, Dubinin–Kaganer–Raduskevich (DKR), Halsey, Harkin–Jura and Flory–Huggins.

Theory

Adsorption kinetics and mechanism

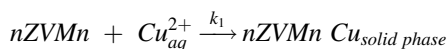
To investigate the reaction mechanism and determine the rate-controlling step of the adsorption of Cu^{2+} onto nZVMn, pseudo first-order, pseudo second-order, Elovich, fractional power and intraparticle diffusion rate equations have been used to model the kinetics of Cu^{2+} adsorption. The quantity of copper uptake at the agitation time, q_t , is given by the expression:

$$q_t = \frac{(C_0 - C_t)V}{W}, \quad (4)$$

C_0 and C_t are the liquid-phase concentrations of the Cu^{2+} solution adsorbate at time 0 and any time t while V and W are the same as defined in Eqs. 2 and 3 above. The experimental data obtained from the optimization of the contact time were tested with kinetic models to study mechanisms of adsorption and the rate-determining step.

The pseudo first-order (Lagergren's rate equation)

Interaction in a solid–liquid system based on the sorption capacity of nZVMn is described by pseudo first order (Lagergren's rate equation). It is assumed that one copper ion is sorbed onto one adsorption site on the nanoscale zerovalent manganese (nZVMn) surface:



The linear form of pseudo first-order equation is generally expressed as:

$$\text{Log}(q_e - q_t) = \text{Log } q_e - \frac{k_1 t}{2.303}, \quad (5a)$$

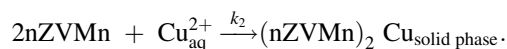
$$h_1 = k_1 q_e, \quad (5b)$$

where q_e is the quantity of Cu^{2+} adsorbed at equilibrium per unit weight of the adsorbent (mg/g), q_t is the amount of Cu^{2+} adsorbed at any time (mg/g), h_1 is pseudo first-order initial adsorption rate and k_1 is the pseudo first-order rate constant (min^{-1}).

The plot of $\text{Log}(q_e - q_t)$ versus t should give a linear relationship and k_1 and q_e can be determined from the slope and intercept of the expression in Eq. 5a, respectively (Ho and McKay 2003).

The pseudo second-order rate equation

The pseudo second-order rate expression has been applied for analysing chemisorption kinetics from liquid solutions (Ho 2004). It is also assumed that copper ion is sorbed onto two adsorption sites on the nZVMn surface according to the interaction between copper ion and nanoscale zerovalent manganese (nZVMn):



The linear form of pseudo second-order rate expression given by the expression:

$$\frac{t}{q_t} = \frac{1}{k_2 q_e^2} + \frac{1}{q_e} t. \quad (6)$$

When t tends to 0, h_2 is defined as:

$$h_2 = k_2 q_e^2. \quad (7)$$

Substituting h_2 into above equation, it becomes:

$$\frac{t}{q_t} = \frac{1}{h_2} + \frac{1}{q_e} t, \quad (8)$$

where h_2 is the initial adsorption rate. If the second-order kinetic equation is applicable, the plot t/q_t against t should give a linear relationship from which the constants k_2 , q_e and h_2 were determined (Ahmad et al. 2014a).

The Elovich model

This is generally described as:

$$dq/dt = \alpha \exp(-\beta q_t). \quad (9)$$

Applying the boundary conditions ($q_t = 0$ at $t = 0$ and $q_t = q_t$ at $t = t$), the simplified form of the Elovich equation is expressed as:

$$q_t = \frac{1}{\beta} \ln(\alpha\beta) + \frac{1}{\beta} \ln(t), \quad (10)$$

where q_t is the amount of adsorbate per unit mass of sorbent at time (t), and α and β are the constants slope and intercept of the determined from the linear plot of q_t versus $\ln(t)$; where α is the initial adsorption rate (mg/g-min) and β is the desorption constant (g/mg) during any one experiment. The slope and intercept are $1/\beta$ and $1/\beta \ln(\alpha\beta)$, respectively. The $1/\beta$ value reflects the number of sites available for adsorption whereas the value of $1/\beta \ln(\alpha\beta)$ indicates the adsorption quantity when $\ln(t)$ equals to zero (Ayanda et al. 2013; Ahmad et al. 2014b).

The fractional power

The fractional power known as power function model can be expressed as:

$$q_t = kt^v. \quad (11)$$

The Eq. 11 above is linearized as:

$$\log(q_t) = \log(k) + v \log(t), \quad (12)$$

where q_t is the amount of adsorbate per unit mass of sorbent, k is a constant, t is time, and v is a positive constant (<1). The parameters v and k were determined from slope and intercept of a linear plot of $\log(q_t)$ versus $\log(t)$ (Ayanda et al. 2013).

Intraparticle diffusivity

The intraparticle diffusion equation is expressed as:

$$q_t = k_{id}t^{0.5} + C, \quad (13)$$

where k_{id} is the intraparticle diffusion rate constant ($\text{mg g}^{-1} \text{min}^{0.5}$) and C is the intercept indicating the thickness of nZVMn. The q_t is the amount of solute adsorbed per unit weight of adsorbent per time (mg/g), and $t^{0.5}$ is the half adsorption time (Boparai et al. 2010; Weber and Morris 1963).

Validity of the kinetic data

The suitability, agreement and best fit among the kinetic models were judged using the statistical validity models such as sum of square error (SSE), Chi-square test (χ^2) and normalized standard deviation (Δq).

The sum of square error (SSE) is the mostly used by researchers. The mathematical expression is given (Foo and Hameed 2010) below:

$$\text{SSE} = \sum_{i=1}^n (q_{e,\text{cal}} - q_{e,\text{exp}})^2. \quad (14)$$

The validity of the kinetic models was also tested using the non-linear Chi-square test. This is a statistical tool necessary for the best fit of an adsorption kinetics system. Better agreement between the experimental data and the calculated quantity adsorbed can be judged using this tool. The mathematical expression is given below:

$$\chi^2 = \sum_{i=1}^n \frac{(q_{e,\text{exp}} - q_{e,\text{cal}})^2}{q_{e,\text{cal}}}. \quad (15)$$

The Chi-square test measures the difference between the experimental and model data, where $q_{e,\text{exp}}$ is experimental quantity adsorbed at equilibrium and $q_{e,\text{cal}}$ is quantity adsorbed calculated from the model equation.

Magnitude of the Chi-square value depends on the agreement between the $q_{e,\text{exp}}$, experimental and the $q_{e,\text{cal}}$, calculated. If data from the model are similar to experimental data, χ^2 will be small and if they differ, χ^2 will be large (Boparai et al. 2010).

The normalized standard deviation Δq_t (%) was calculated using Eq. 16 below (Bello et al. 2014):

$$\Delta q (\%) = 100 \frac{\sqrt{\sum_{i=1}^n \left(\frac{q_{e,\text{exp}} - q_{e,\text{cal}}}{q_{e,\text{exp}}} \right)^2}}{n - 1}, \quad (16)$$

where n is the number of data points and other parameters are the same as earlier defined. Lower value of Δq_t indicates a good fit between experimental and calculated data (Bello et al. 2014).

Adsorption isotherm model

An adsorption isotherm is an expression that relates the amount of substance adsorbed per unit mass of the adsorbent to the equilibrium concentration at constant temperature (Foo and Hameed 2010).

Freundlich isotherm model

The Freundlich adsorption isotherm gives an expression encompassing the surface heterogeneity and the exponential distribution of active sites and their energies. The linear form of Freundlich equation is (Ahmad et al. 2014c; Boparai et al. 2010).

$$\log Q_e = \log K_f + \frac{1}{n_f} \log C_e. \quad (17)$$

The Freundlich isotherm constants, K_f and n_f indicating the adsorption capacity and intensity, respectively, are parameters characteristic of the adsorbent–adsorbate system determined from the intercept and slope of the plot of $\log Q_e$ against $\log C_e$.

Langmuir isotherm model

Langmuir adsorption isotherm assumes a monolayer adsorption onto a homogeneous surface with a finite number of identical sites. There is uniform energy of adsorption onto the surface and no transmigration of adsorbate in the plane of the surface (Ho 2004; Foo and Hameed 2010). The linear form of Langmuir represents:

$$\frac{C_e}{Q_e} = \frac{1}{K_L Q_{\text{max}}} + \frac{C_e}{Q_{\text{max}}}. \quad (18)$$

Q_{max} is the maximum monolayer coverage capacity (mg g^{-1}), K_L is the Langmuir isotherm constant (L mg^{-1}) related to the energy of adsorption. The

essential features of the Langmuir isotherm may be expressed in terms of equilibrium parameter R_L , which is a dimensionless constant referred to as separation factor:

$$R_L = \frac{1}{1 + K_L C_o}. \quad (19)$$

R_L value indicates the adsorption nature to either unfavourable or unfavourable.

Temkin isotherm model

Temkin isotherm contains a factor that explicitly taking into the account of adsorbent–adsorbate interactions. The model assumes that heat of adsorption (function of temperature) of all molecules in the layer would decrease linearly with the surface coverage due to adsorbent–adsorbate interactions. The linear form of the equation is given as (Boparai et al. 2010; Temkin 1940):

$$Q_e = \frac{RT}{b_T} \ln A_T + \frac{RT}{b_T} \ln C_e, \quad (20)$$

where $B = RT/b_T$, b_T is the Temkin isotherm constant related to the heat of adsorption and A_T is the Temkin isotherm equilibrium binding constant ($L g^{-1}$). The values of these constants were determined from the slope and intercept obtained from appropriate plot of Q_e versus $\ln C_e$.

Dubinin–Kaganer–Radushkevich (DKR) isotherm model

DKR isotherm model is generally applied to express the adsorption mechanism with a Gaussian energy distribution onto a heterogeneous surface. The model has often successfully fitted high solute activities and the intermediate range of concentrations data well. The linear equation is given as:

$$\ln Q_e = \ln Q_d - A_{DKR} \varepsilon^2, \quad (21)$$

where A_{DKR} is the DKR isotherm constant (mol^2/kJ^2) related to free adsorption energy and Q_d is the theoretical isotherm saturation capacity (mg/g). The values of A_{DKR} and Q_d were determined, respectively, from the slope and intercept of the plot of $\ln Q_e$ versus ε^2 . The parameter ε is the Polanyi potential which is computed as:

$$\varepsilon = RT \ln \left[1 + \frac{1}{C_e} \right]. \quad (22)$$

The approach was usually applied to distinguish the physical and chemical adsorption of metal ions with its mean adsorption free energy, E per molecule of adsorbate (for removing a molecule from its location in the adsorption space to the infinity) can be computed by the relationship (Bello et al. 2014):

$$E = - \left[\frac{1}{\sqrt{2A_{DKR}}} \right]. \quad (23)$$

Halsey isotherm model

Halsey isotherm is used to evaluate the multilayer adsorption at a relatively large distance from the surface. The Halsey isotherm model is expressed as (Song et al. 2014; Bhatt and Shah 2013 and Basar 2006).

$$\ln q_e = \left[\left(\frac{1}{n_H} \right) \ln K \right] - \left(\frac{1}{n_H} \right) \ln C_e. \quad (24)$$

A plot of $\ln q_e$ against $\ln C_e$ should give a linear graph and the Halsey constants K_H and n_H were determined from the intercept and slope, respectively.

Harkin–Jura isotherm model

The isotherm equation also accounts for multilayer adsorption and can be explained by the existence of heterogeneous pores distribution (Basar 2006; Harkins and Jura 1944). The Harkin–Jura isotherm model is expressed as (Song et al. 2014; Bhatt and Shah 2013):

$$\frac{1}{q_e^2} = \frac{B_{HJ}}{A_{HJ}} - \frac{1}{A_{HJ}} \log C_e. \quad (25)$$

The plot of $\frac{1}{q_e^2}$ versus $\log C_e$ should give a straight line hence the Harkin–Jura constants, A_{HJ} and B_{HJ} , were determined from the slope and intercept of the linear plot.

Flory–Huggins isotherm model

This is generally used to account for the surface coverage of the adsorbate on the adsorbent. The non-linear and its near expressions are given below (Foo and Hameed 2010; Febrianto et al. 2009):

$$\frac{\theta}{C_o} = K_{FH} (1 - \theta)^{n_{FH}}, \quad (26)$$

$$\log \left(\frac{\theta}{C_o} \right) = \log K_{FH} + n_{FH} \log (1 - \theta), \quad (27)$$

where $\theta = 1 - \left(\frac{C_e}{C_o} \right)$, θ is the degree of surface coverage, n_{FH} and K_{FH} are Flory–Huggin's constants defined as the number of metal ions occupying adsorption sites and the equilibrium constant of adsorption, respectively. They can be determined from the linear plot of $\log(\theta/C_o)$ versus $\log(1 - \theta)$.

Thermodynamic studies

The data obtained from the effect of temperature at the equilibrium studies were tested with the adsorption

thermodynamic equations. The thermodynamic parameters can be determined using equations below (Ayanda et al. 2013; Boparai et al. 2010):

$$K_c = \frac{q_e}{C_e}, \quad (28)$$

$$\log K_c = \frac{\Delta S^\circ}{2.303R} - \frac{\Delta H^\circ}{2.303RT}. \quad (29)$$

The Van't Hoff plot of $\log K_c$ versus $1/T$ should give a straight line and the thermodynamic parameters, standard enthalpy change ΔH° (kJ mol⁻¹) and standard entropy change ΔS° (J mol⁻¹ K⁻¹) were determined from the slope and intercept of Eq. 29, respectively. The standard Gibbs free energy ΔG° (KJ mol⁻¹) was calculated using the Eq. 30:

$$\Delta G = -2.303 RT \log K_c. \quad (30)$$

Results and discussion

Characterization of nZVMn

Physicochemical properties of nZVMn

Table 1 below summarizes the physicochemical properties of nanoscale zerovalent manganese. The pH of point of zero charge (pH_{PZC}) is defined as the pH at which the surface of nZVMn has a net neutral charge. The pH_(PZC) of nZVMn was determined by salt addition method. The significance of this is that nZVMn has negative charge at solution pH values greater than the pzc and thus a surface

Table 1 Physicochemical parameters of nZVMn

Characteristics	nZVMn
PZC	5.01
Surface area	
BET surface area	131.3490 m ² /g
<i>t</i> Plot micropore area	11.3063 m ² /g
<i>t</i> Plot external surface area	120.0427 m ² /g
BJH adsorption cumulative surface area of pores	
Between 17.000 and 3000.000 Å diameter	132.073 m ² /g
Pore volume	
Single point adsorption total pore volume of pores	
Less than 973.808 Å diameter at $P/P_o = 0.979706513$	0.559789 cm ³ /g
<i>t</i> Plot micropore volume	0.003846 cm ³ /g
BJH adsorption cumulative volume of pores	
Between 17.000 and 3000.000 Å diameter	0.611320 cm ³ /g
Pore size	
Adsorption average pore width (4 V/A by BET)	170.4736 Å
BJH adsorption average pore diameter (4 V/A)	185.147 Å

on which cations adsorb. The pH of nZVMn is 5.01 indicating that nZVMn was suitable for the adsorption of Cu²⁺ at a pH above 5.01 (Jaafar et al. 2013; Srivastava et al. 2005).

From the BET result (Table 1), the surface area of nZVMn is 131.3490 m²/g, *t* plot micropore area is 11.3063 m²/g, *t* plot external surface area is 120.0427 m²/g. The BJH adsorption cumulative surface area of pores between 17.000 and 3000.000 Å diameter is 132.073 m²/g. The single point adsorption total pore volume of pores less than 973.808 Å diameter at $P/P_o = 0.979706513$ is 0.559789 cm³/g. *t* plot micropore volume is 0.003846 cm³/g. The BJH adsorption cumulative volume of pores between 17.000 and 3000.000 Å diameter is 0.611320 cm³/g. The adsorption average pore width (4 V/A by BET) is 170.4736 Å. The BJH adsorption average pore diameter (4 V/A) is 185.147 Å. The relatively higher value of the external surface area compared to the micropore surface area implies that nZVMn utilized its external surface for adsorption than its micropore.

UV–VIS analysis

The reduction of Mn²⁺ to Mn⁰ (nZVMn) by sodium borohydride was monitored using a Beckmann Coulter DU 730 Life Science UV–VIS spectrophotometer. A small aliquot was drawn from the reaction mixture and a spectrum was taken at a wavelength from 200 to 800 nm.

The adsorption spectrum of nZVMn as presented in Fig. 1 showed the maximum wavelength was observed at about 380 nm. This is an indication of surface plasmon resonance which is the collective oscillation of the conduction of electron in resonance with light due to electron conferment in nZVMn. The SPR depends mainly on the nature of the metal, the morphology of the nanoparticles and the dielectric properties of the environment or medium of dispersion (Jain et al. 2007; Waghmare et al. 2011).

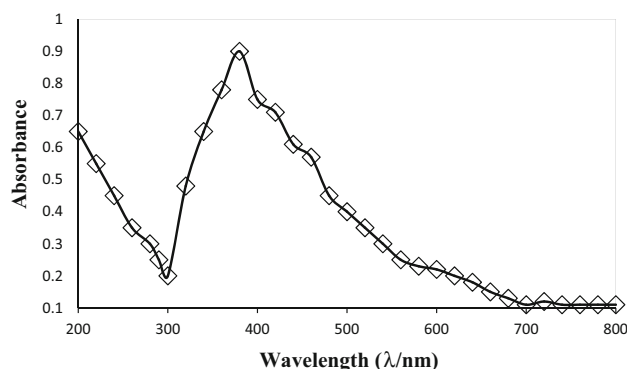
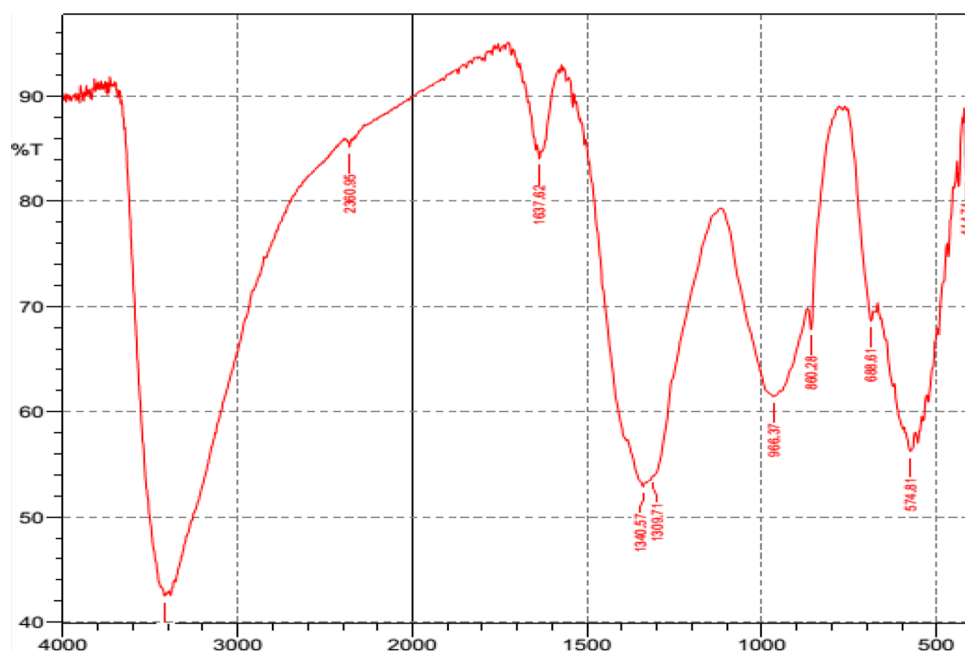


Fig. 1 UV–VIS spectrum of nZVMn

Fig. 2 FT-IR spectrum of nZVMn

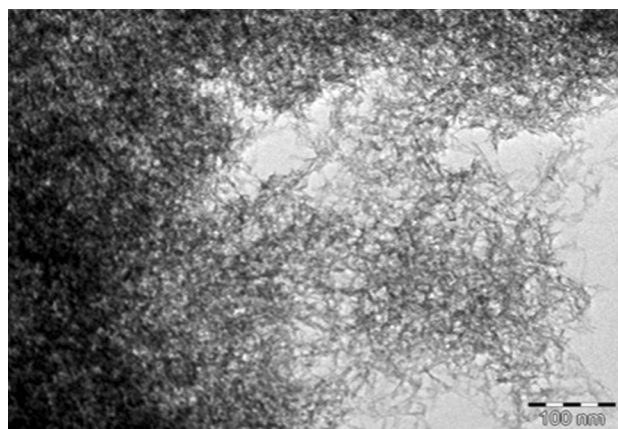
FTIR analysis

Figure 2 below presents FTIR spectrum of manganese nanoparticles with some characteristic vibration bands at 3288, 1636, 1307, and 504 cm^{-1} . The peak at 3288 cm^{-1} stands for O–H broad of alcohol from the medium of dispersion of nZVMn where the manganese nanoparticle was kept for preservation, H–O–H stretching (1636 cm^{-1}), C–O stretching of alcohol at 1309 cm^{-1} and the peak at 504 cm^{-1} corresponds to nZVMn as summarized in Table 2 below (Sinha et al. 2011; Li et al. 2009).

TEM analysis

TEM micrograph in Fig. 3 reveals the micro-images of nanoscale zerovalent manganese (nZVMn) of size range 6.120–99.428 nm.

The traces of dispersions and whiskers which are attributes of manganese nanoparticles were observed. This is in agreement with the finding of Lisha et al. 2010.

**Fig. 3** TEM of nZVMn**Table 2** Summary of the functional groups and vibration frequencies on the IR spectrum of nZVMn

Functional group	Vibration bands (cm^{-1})
O–H str of alcohol	3288
H–O–H str	1636
–C–O	1309
nZVMn	504

Effect of ZVMn dose, agitation speed and contact time

Optimization of the amount of zerovalent manganese nanoparticles needed for the adsorption of Cu^{2+} was carried out. It was observed that the percentage of Cu^{2+} removed increased with an increase in the adsorbent dose. The removal efficiency increased from 91.6 % at 50 mg to 100 % at 100 mg due to an increase in the number of available adsorption sites and large surface area of nZVMn as shown in Fig. 4. The adsorbent (nZVMn) became saturated with Cu^{2+} and the residual concentrations increased at adsorbent dose less than 100 mg until a saturated point was reached. Above 100 mg, there was relatively no significant increase in the quantity adsorbed because all the

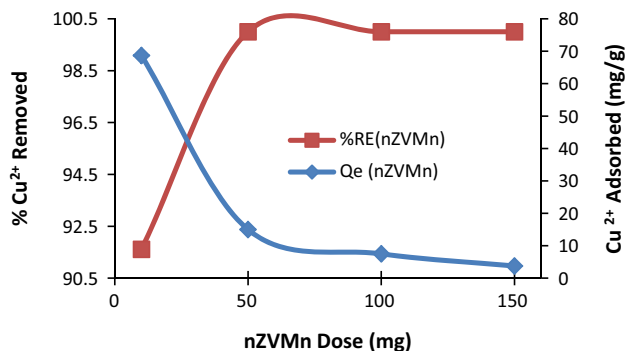


Fig. 4 Effect of nZVMn dose on Cu²⁺ adsorbed by nZVMn. Experimental conditions: optimum Cu²⁺ concentration = 100 ppm; volume of Cu²⁺ solution = 50 mL; pH = 5, stirring speed = 200 rpm, contact time = 60 min, and temperature = 25 ± 2 °C

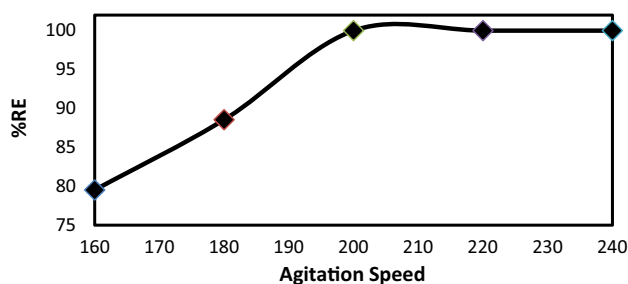


Fig. 5 Effect of agitation speed on Cu²⁺ adsorbed onto nZVMn. Experimental conditions: optimum Cu²⁺ concentration = 100 ppm; volume of Cu²⁺ solution = 50 mL; nZVMn dose = 100 mg; pH = 5, contact time = 60 min, and temperature = 25 ± 2 °C

active sites had been saturated and the quantity adsorbed decreased. This finding is in agreement with the reports of Hao et al. (2010); Srivastava et al. (2005).

Agitation speed (Fig. 5) plays an important role in adsorption studies because it promotes turbulence, frequency of collision and improves mass transfer in the medium between the two phases (Larous et al. 2005). To optimize agitation speed, five different speeds were chosen between 160 and 240 rpm, as shown in Fig. 5. It was observed that removal efficiency increased from 79.52 % to 100 % with an increase in the agitation speed. It increased until maximum removal efficiency was obtained at 200 rpm above which there was no significant increase. Other adsorption studies were carried out at this optimum agitation speed. This finding is in agreement with the report of Ayanda et al. 2013.

Contact time (Fig. 6) is another important factor in all transfer phenomena such as adsorption. A short contact time to reach equilibrium indicates the fast transport of metal ions from the bulk to the outer and inner surface of nZVMn. In addition, contact time also controls the buildup of charges at the solid–liquid interfaces and for this reason,

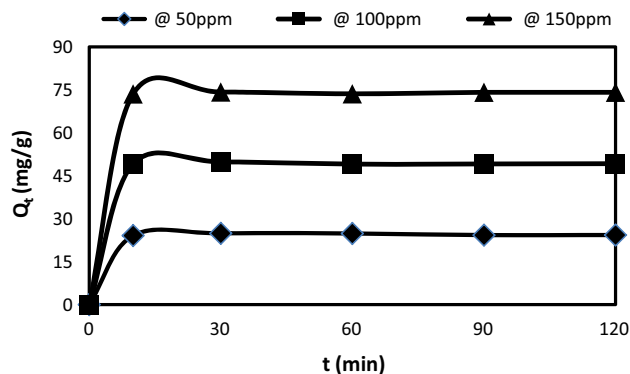


Fig. 6 Effect of contact time on Cu²⁺ adsorbed onto nZVMn. Experimental conditions: Cu²⁺ concentration = 100 ppm; volume of Cu²⁺ solution = 50 mL; nZVMn dose = 100 mg; pH = 5, stirring speed = 200 rpm, and temperature = 25 ± 2 °C

optimization of the effect of contact time on the adsorption of Cu²⁺ onto nZVMn was investigated at three different concentrations 50 ppm, 100 ppm and 150 ppm from 10 min to 120 min. The rate of adsorption and equilibrium was attained between 30 and 60 min with 39.85, 59.76 and 99.2 mg/g quantity adsorbed as shown in Fig. 6. The optimum contact time observed was 60 min after which as steady-state approximation set in and a quasi-equilibrium situation was attained (Srivastava et al. 2005). All other operational parameters were studied at 60-min contact time.

Adsorption kinetics and mechanism of reaction

The kinetic studies vis-à-vis pseudo first-order, pseudo second-order, Elovich, Fractional power, intraparticle diffusion plots are shown in Figs. 7, 8, 9, 10 and 11,

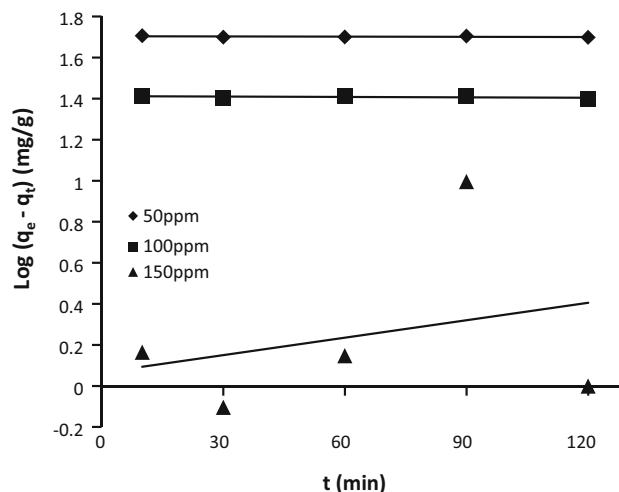


Fig. 7 Pseudo first-order kinetics plot for sorption of Cu²⁺ onto nZVMn

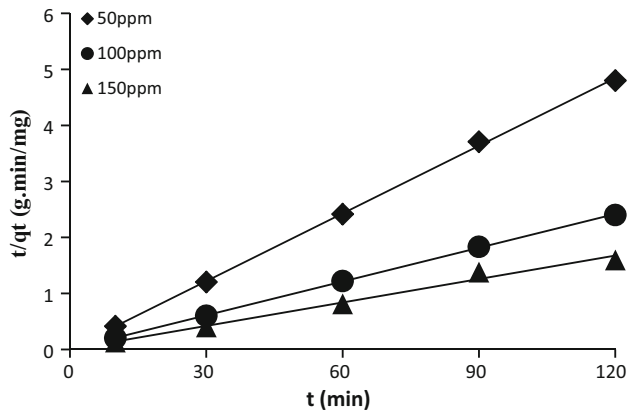


Fig. 8 Pseudo second-order kinetics plot for sorption of Cu^{2+} onto nZVMn

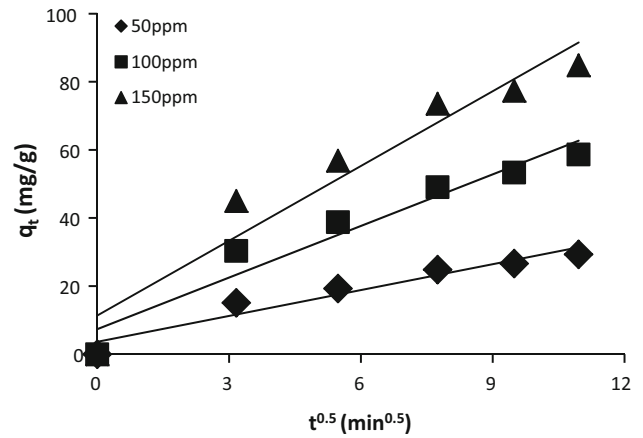


Fig. 11 Intraparticle diffusion plot for sorption of Cu^{2+} onto nZVMn

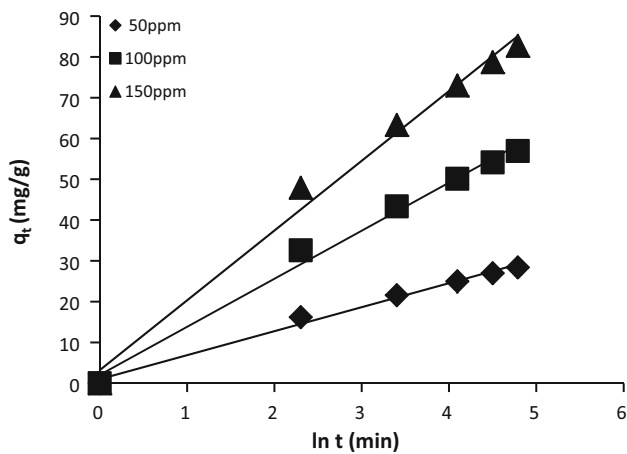


Fig. 9 Elovich kinetics model plot for sorption of Cu^{2+} nZVMn

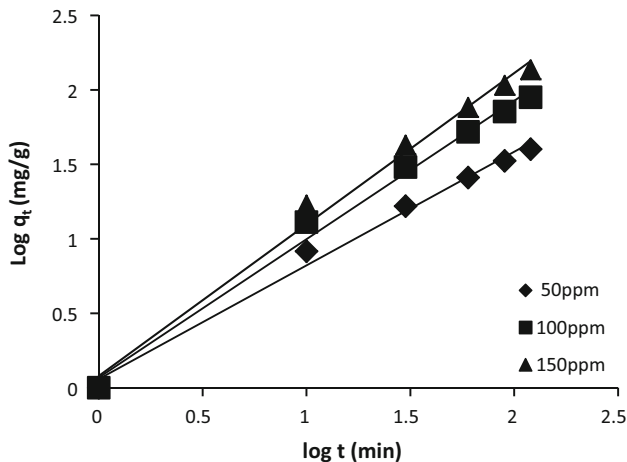


Fig. 10 Fractional power rate equation plot for onto Cu^{2+} onto nZVMn

respectively. The evaluated parameters from these kinetic models are well stated in Table 3. From the regression coefficient (R^2) point of view, the adsorption kinetics data were well described by pseudo second-order kinetics having $R^2 > 0.99$ (Fig. 8). Considering Table 3, the rate of reaction, h_2 for pseudo second order was distinctly higher than that of pseudo first order. The experimental quantity adsorbed and the calculated quantity adsorbed ($q_{e,exp}$ and $q_{e,cal}$) from pseudo second-order kinetics were in close agreement suggesting that the kinetic data from the adsorption of Cu^{2+} fitted well to pseudo second-order model.

Shown in Fig. 9 is the linear plot of Elovich model. This model describes adsorption on highly heterogeneous adsorbent (Hao et al. 2010). The values of α (adsorption rate) (Table 3) increase with an increase in concentration as a result of increase in the number of sites. The values $1/\beta$ at 50 ppm, 100 and 150 ppm are 5.882, 11.764 and 17.123, respectively. These values reflected the number of sites available for adsorption (Ahmad et al. 2014b, Song et al. 2014).

The parameters of fractional power (Fig. 10) were evaluated at different concentrations from the plot of $\log(q_t)$ versus $\log(t)$ in Eq. 12 and the values of R^2 (0.991, 0.991 and 0.989) showed that the kinetic data fitted also well to the fractional power model.

Adequate understanding of the adsorption mechanism is enhanced by the determination of the rate-controlling/determining step. The three definite steps that could be used to describe the adsorption rate are (Boparai et al. 2010; Chingombe et al. 2006): (1) Intraparticle or pore diffusion, where adsorbate molecules percolates into the interior of adsorbent particles, (2) liquid film or surface diffusion where the adsorbate is transported from the bulk solution to

Table 3 Kinetics model parameters for the sorption of different initial concentrations Cu^{2+} onto nZVMn

Kinetics model parameters	Initial metal ion concentrations		
	50 ppm	100 ppm	150 ppm
Pseudo first order			
q_e , exp (mg/g)	24.843	49.069	73.593
q_e , cal (mg/g)	50.606	25.823	1.163
k_1 (min^{-1})	6.909×10^{-5}	1.612×10^{-4}	0.0645
h_1 (mg/g/min)	3.496×10^{-3}	4.163×10^{-3}	0.075
R^2	0.169	0.145	0.0831
SSE	663.73	540.376	5246.11
χ^2	13.116	20.926	4510.838
Δq	20.741	9.475	19.684
Pseudo second order			
q_e , exp (mg/g)	24.843	49.069	73.593
q_e , cal (mg/g)	24.813	49.751	71.942
k_2 (g/mg/min)	0.1299	0.05386	0.00254
h_2 (mg/g/min)	79.977	133.332	15.288
R^2	0.999	0.999	0.986
SSE	0.0009	0.465	2.726
χ^2	3.627×10^{-5}	9.3490×10^{-3}	3.823×10^{-2}
Δq	0.024	0.278	0.449
Elovich			
α ($\text{g min}^2/\text{mg}$)	6.696	13.996	20.668
β ($\text{g min}/\text{mg}$)	0.17	0.085	0.0584
R^2	0.991	0.991	0.986
SSE	0.0557	1.449	0.122
χ^2	2.22×10^{-3}	2.88×10^{-2}	1.66×10^{-2}
Δq	0.189	0.491	0.0948
Fractional power			
ν (min^{-1})	0.764	0.93	1.017
k_3 (mg/g)	1.142	1.17	1.199
$k_3\nu$ (mg/g/min)	0.872	0.158	1.22
R^2	0.991	0.991	0.99
SSE	1.383	12.559	13.374
χ^2	0.053	0.239	0.0172
Δq	0.056	1.444	0.994
Intraparticle diffusion			
k_{ip} (mg/g/min ^{0.5})	2.534	5.054	7.323
C	3.646	7.357	11.34
R^2	0.937	0.937	0.927
SSE	2.462	6.579	30.548
χ^2	0.106	0.141	0.449
Δq	1.982	1.045	1.502

the external surface of adsorbent, and (3) adsorption on the interior sites of the sorbent. Since the rate of reaction from the pseudo second order is very high, it shows that the adsorption rate was very fast and hence it is assumed that it

does not only influence the overall kinetics. The rate of adsorption could also be controlled by intraparticle. The Weber–Morris intraparticle diffusion model has often been used to verify if intraparticle diffusion is the rate-limiting step (Igwe et al. 2005). In this study, the intraparticle diffusion (Fig. 11) shows a linear plot of (q_t) versus ($t^{0.5}$) from Eq. 13 where k_{id} (intraparticle diffusion rate constant) and C (thickness of the surface) were determined from the slope and intercept. The intercept which is the thickness of the surface gave information about contribution of the surface adsorption in the rate-determining step. The larger the intercept, the greater is its contribution. The linear plot of q_t versus $t^{1/2}$ suggested that adsorption of Cu^{2+} was governed by pore diffusion. Since the plot of q_t versus $t^{0.5}$ did not pass through the origin, it indicated that intraparticle is not the only rate-determining step (Ahmad et al. 2014c; Igwe and Abia 2006; Wu et al. 2001). It is suggested that other steps like external diffusion and liquid film diffusion may be involved in the rate-determining steps.

A strong confirmation that the adsorbate (Cu^{2+}) had percolated into the pores and surface of the nZVMn was provided by the SEM and EDX analyses shown in Fig. 12a–d. The morphological characterization was done before and after adsorption of Cu^{2+} onto nZVMn. Figure 12a depicts the SEM micrograph of zerovalent manganese nanoparticle before adsorption. Before adsorption, SEM spectrum reveals coarse, rough and crake surface which is an indication of high surface area and presence of pores for uptake of Cu^{2+} . The presence of cracks surface enhanced free and dynamic flow of the adsorbate into the pores of nZVMn. Also, the rough and coarseness of the surface indicating a higher surface area facilitated strong adsorption of Cu^{2+} into the pores and external surface of nZVMn nano-adsorbent (Morsali et al. 2011). The SEM (Fig. 12b) micrograph after adsorption reveals that the surface of the nano-adsorbent had changed, the traces of cracks were finally eliminated by the flow of Cu^{2+} solution. The Cu^{2+} had percolated on the surface of nZVMn and evidence is seen by the robust nature of the nZVMn after adsorption.

The EDX spectra (Fig. 12c–d) give information on the surface atomic distribution and the chemical elemental composition of nZVMn. Figure 12c shows the prominent peaks of manganese nanoparticles and at 0.8 and 6.0 keV energy dispersions. The presence of copper before adsorption arose from the copper grid used during the analysis, other elements may arise from the traces of additives used during the analysis. Nevertheless, the presence of copper as shown in Fig. 12d came from the Cu^{2+} solution (Sinha et al. 2011; Waghmare et al. 2011; Lisha et al. 2010).

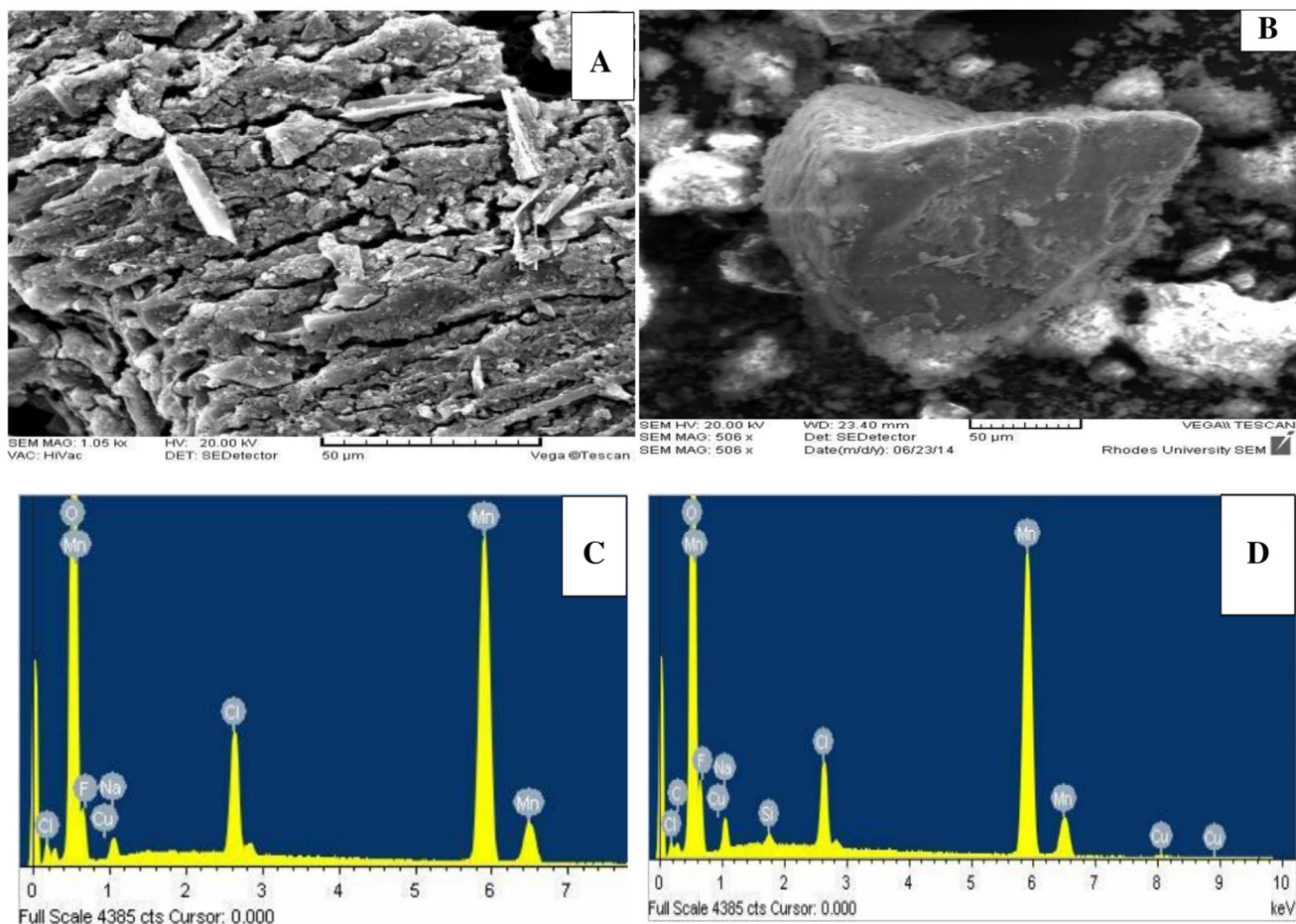


Fig. 12 (a) SEM image of nZVMn before sorption (b) SEM image of nZVMn after sorption (c) EDX spectrum of nZVMn before sorption, (d) EDX spectrum of Cu(II) loaded nZVMn after sorption

Validity test on the kinetics data

The kinetics data were validated using three statistical models namely: sum of square error (SSE), Chi-square test (χ^2), and normalized standard deviation (Δq). The evaluated data are also summarized in Table 3. The applicability of these kinetics models (pseudo first order, pseudo second order, Elovich, fractional power and intraparticle diffusion) was judged by comparing the R^2 values with SSE, Chi-square (χ^2) and normalized standard deviation (Δq) %. The closer the value of R^2 to unity, the lower the value of SSE, χ^2 and Δq , the better the model in describing the adsorption of Cu^{2+} onto nZVMn. Pseudo second order perfectly fitted to this while poor description was obtained in pseudo first-order parameters. This finding is supported by the report from the literature (Ahmad et al. 2014a, b, c; Bello et al. 2014; Song et al. 2014; Bhatt and Shah 2013; Hao et al. 2010; Foo and Hameed 2010).

Effect of pH

Effect of pH plays one of the greatest roles in the adsorption studies because it influences the surface charge of the adsorbents, ionic mobility, the degree of ionization and speciation of different pollutants and solution chemistry of contaminants (i.e. hydrolysis, redox reactions, polymerization and coordination) (Ren et al. 2008). It has been reported that Cu(II) in aqueous solution exists in different forms such as Cu^{2+} , $\text{Cu}(\text{OH})^+$, $\text{Cu}(\text{OH})_2$, $\text{Cu}(\text{OH})_3^-$ and $\text{Cu}(\text{OH})_4^{2-}$ and the predominant copper species at pH < 6.0 is Cu^{2+} (Badruddoza et al. 2011; Xu et al. 2006).

Optimum pH was attained at 5 with the percentage removal >99 %. However, at lower pH between 1 and 3, in acidic medium, protonation occurs and electrostatic competition sprout up between Cu^{2+} and other protonated species like H^+ for the available adsorption sites. This competition reduced as soon as the pH approaches neu-

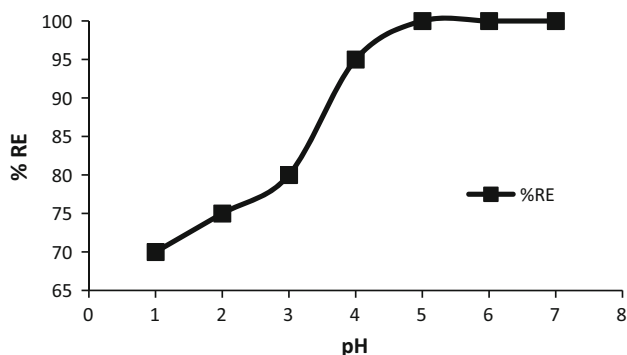


Fig. 13 Effect of pH on Cu^{2+} adsorbed onto nZVMn. Experimental conditions: optimum Cu^{2+} concentration = 100 ppm; volume of Cu^{2+} solution = 50 mL; nZVMn dose = 100 mg; stirring speed = 200 rpm, contact time = 60 min

trality and tending towards alkaline medium where deprotonation occurs. At this point, percentage of Cu^{2+} removed increase because the competition for the available adsorption sites had reduced. Maximum values of the percentage and the quantity removed were observed at pH 5 (Fig. 13). This is supported by the finding of Badruddoza et al. 2011; Xiao et al. 2011; Kara and Demirbel 2012; Cai et al. 2014; Sikdera et al. 2014; Gong et al. 2012; Cho et al. 2012; Karabellia et al. 2011; White et al. 2009; Zhou et al. 2009; Huang and Chen 2009; Doğan et al. 2009).

Adsorption isotherm

The effect of initial concentration as shown in Fig. 14 was studied from 10 to 200 ppm. At a lower concentration, the percentage removal efficiency increases because of the availability of more active sites until the adsorption sites are saturated at 100 ppm above which there was no significant increase in the quantity adsorbed and percentage removal efficiency. The increase in adsorption capacity

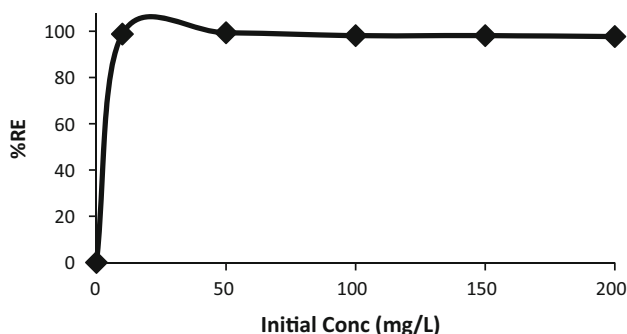


Fig. 14 Effect of initial concentration on Cu^{2+} adsorbed onto nZVMn. Experimental conditions: optimum Cu^{2+} concentration = 100 ppm; volume of Cu^{2+} solution = 50 mL; nZVMn dose = 100 mg; pH = 5, contact time = 60 min, and temperature = 25 ± 2 °C

from 4.935 to 93.737 mg/g with an increase in initial Cu^{2+} concentration from 10 to 200 ppm was as a result of the increase in driving force due to the concentration gradient developed between the bulk solution and surface of the nZVMn nano-adsorbent (Kumar et al. 2010). At higher Cu^{2+} concentrations, the active sites of the adsorbents were surrounded by more Cu^{2+} and the process of adsorption continued until equilibrium was reached.

The adsorption isotherms provide information and insight into the relationship between the adsorbate and the adsorbent. In this research, adsorption data were tested with seven different isotherms models: Langmuir, Freundlich, Temkin, DKR, Halsey, Harkin–Jura, Flory–Huggins as shown in Figs. 15, 16, 17, 18, 19, 20 and 21. The summary of the evaluated parameters and the correlation coefficients are stated in Table 4. Based on the correlation coefficients, the equilibrium adsorption data fitted better into Freundlich, Langmuir, Temkin, DRK and Halsey models. Figure 15 shows the Freundlich plot for adsorption of Cu^{2+} onto nZVMn. The constants K_F and n were determined from the plot of $\log Q_e$ versus $\log C_e$. $1/n$ is a heterogeneity parameter. In this study, the value of n (Table 4) is 1.352 which is less than 10 indicating a favourable adsorption (Foo and Hameed 2010).

The Langmuir constants (Fig. 16a; Table 4), Q_{\max} (maximum monolayer coverage capacity), and K_L (Langmuir isotherm constant related to the energy of adsorption) were determined from the linear plot of C_e/Q_e against C_e in Eq. 18.

The essential feature of the Langmuir isotherm may be expressed in terms of equilibrium parameter R_L (Fig. 16b) which is a dimensionless constant referred to as separation factor or equilibrium parameter (Hao et al. 2010). The value of R_L is an important indicator to determine if adsorption will be favourable or unfavourable. If $R_L > 1$, it is unfavourable, if $R_L = 1$, it is linear, if $0 < R_L < 1$ it is favourable and irreversible if $R_L = 0$. The values of R_L

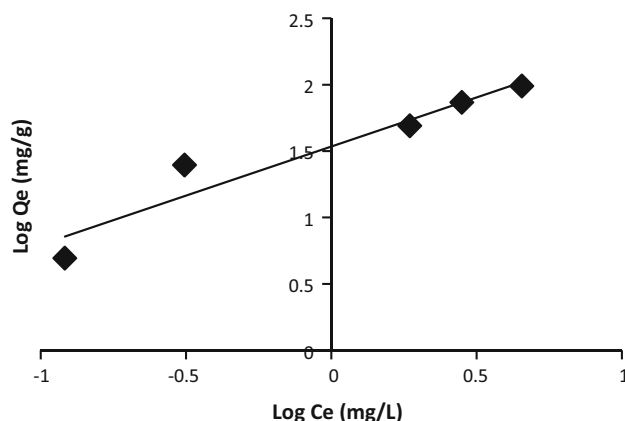


Fig. 15 Freundlich isotherm model for sorption of Cu^{2+} onto nZVMn

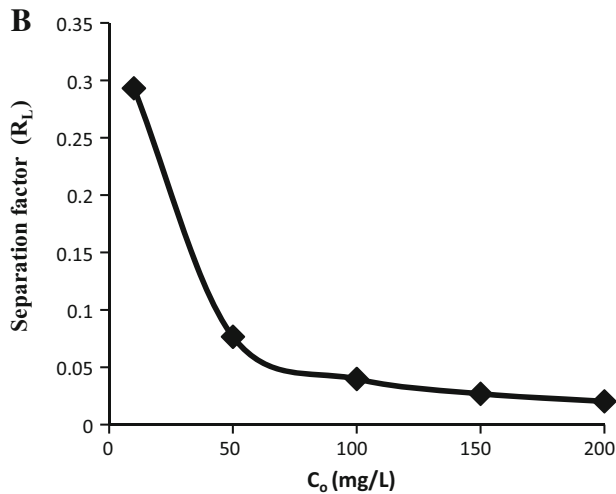
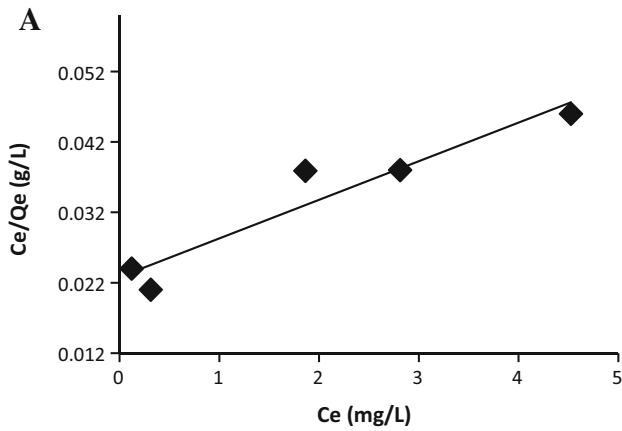


Fig. 16 **a** Langmuir isotherm model for sorption of Cu^{2+} onto nZVMn, **b** separation factor on sorption of Cu^{2+} onto nZVM

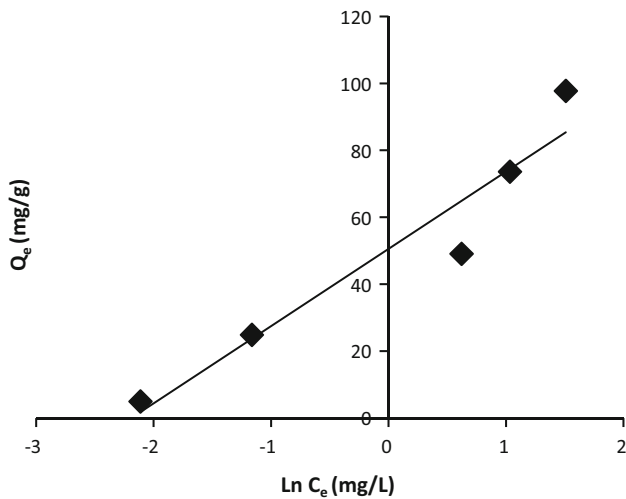


Fig. 17 Temkin isotherm model for sorption of Cu^{2+} onto nZVMn

(Fig. 16b; Table 4) from this research range from 2.03×10^{-2} to 2.93×10^{-1} which is less than unity indicating a favourable adsorption.

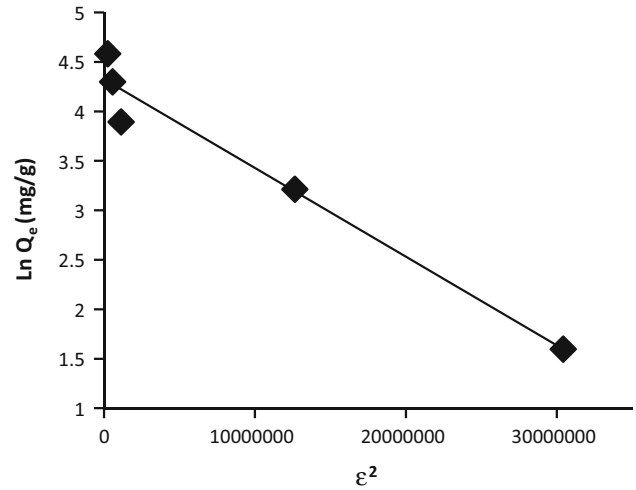


Fig. 18 DKR isotherm model for sorption of Cu^{2+} onto nZVMn

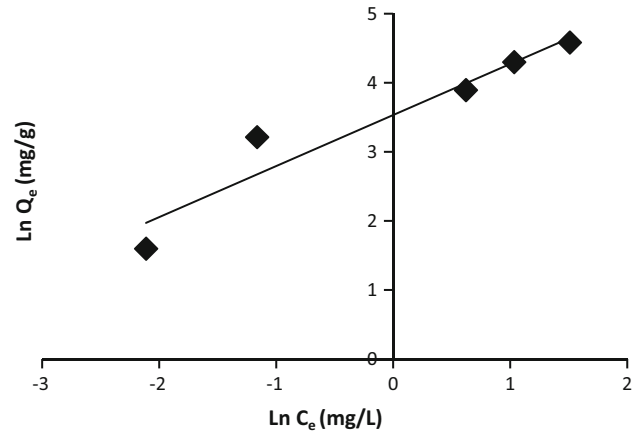


Fig. 19 Halsey isotherm model for sorption of Cu^{2+} onto nZVMn

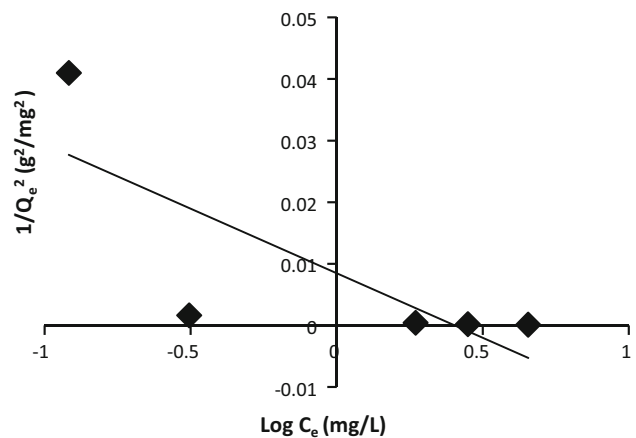


Fig. 20 Harkin–Jura isotherm model for sorption of Cu^{2+} onto nZVMn

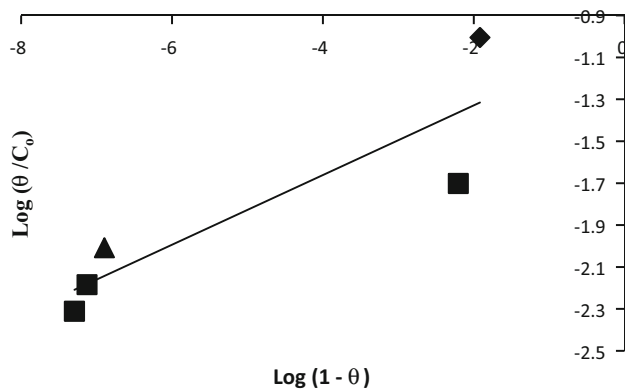


Fig. 21 Flory–Huggins isotherm model for sorption of onto nZVMn

Table 4 Langmuir, Freundlich, Temkin, DKR, Halsey, Harkin–Jura and Flory–Huggins isotherm models parameters and correlation coefficients for adsorption of copper ions onto nZVMn particles

Isotherm models	Parameters	Cu ²⁺
Freundlich	k_f	90.824
	$1/n_F$	0.739
	n_F	1.352
	R^2	0.921
Langmuir	Q_{max} (mg g ⁻¹)	181.818
	K_L (L mg ⁻¹)	0.241
	R_L (× 10 ⁻¹)	0.203–2.93
	R^2	0.911
Temkin	b_T (J mol ⁻¹)	107.352
	β (Lg ⁻¹)	23.079
	A_T (Lg ⁻¹)	8.934
	R^2	0.925
DRK	Q_d	75.467
	A_{DRK}	9×10^{-8}
	E (KJ/mol)	2.357
	R^2	0.967
Halsey	$1/n$	-0.739
	n_H	-1.352
	K_H	8.416×10^{-3}
	R^2	0.921
Harkin–Jura	$1/A_{H-J}$	0.021
	A_{H-J}	47.619
	B	0.405
	R^2	0.605
Flory–Huggins	n_{FH}	0.166
	K_{FH}	0.101
	R^2	0.779

The copper adsorption capacity on nZVMn is 181.818 mg g⁻¹ (Table 5). This is much higher compared to other nano-adsorbents reported in the literature such as stated in Table 5. This high adsorption capacity is due to

high BET surface area. Based on the comparison between zerovalent manganese nanoparticle (nZVMn) and other nano-adsorbents previously used in adsorption of Cu²⁺ (Table 5), nZVMn can be enlisted among novel and promising adsorbents (Hao et al. 2010).

Figure 17 depicts the linear plot of Temkin isotherm model for adsorption of Cu²⁺ onto nZVMn. The Temkin isotherm constant, b_T , related to the heat of adsorption and the Temkin isotherm equilibrium binding constant (A_T) (L g⁻¹) were determined from the slope and intercept as 107.352 J mol⁻¹ and 8.934 L g⁻¹, respectively. Observation from Table 4 shows that the R^2 values of Temkin and Langmuir are close.

The adsorption data also fitted well into DKR model based on R^2 value (Fig. 18, Table 4). Since the magnitude of E (free energy of transfer of one solute from infinity to the surface of nZVMn) is less than 8 kJ mol⁻¹, the adsorption mechanism was physisorption which further supported Freundlich Isotherm. This finding is supported by the report of Song et al. (2014) and Lisha et al. (2010).

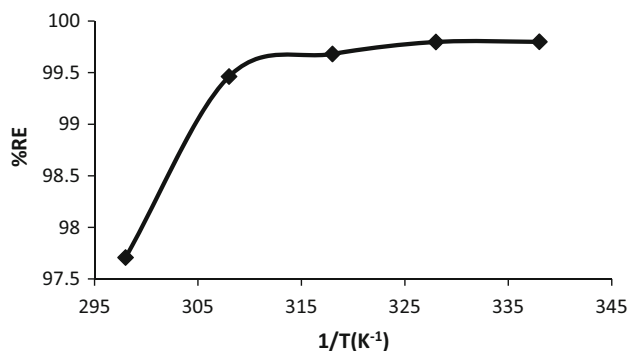
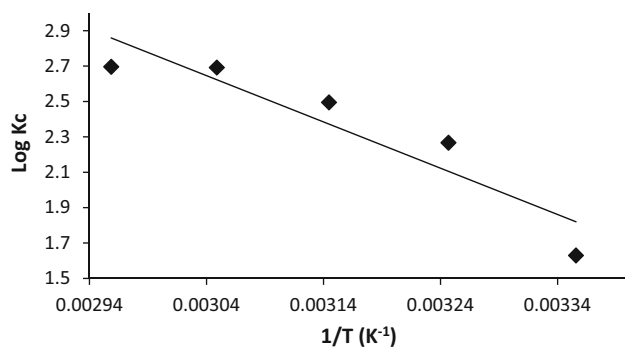
The adsorption data also fitted well to Halsey isotherm model (Fig. 19) with $R^2 = 0.921$ (Table 4) to further support the prevalence of multilayer adsorption process. Only Harkin–Jura (Fig. 20) and Flory–Huggins (Fig. 21) poorly described the adsorption process and this was confirmed with their low R^2 values in Table 4.

Thermodynamic studies

Temperature is another important parameter in the adsorption studies because some important thermodynamic parameters like enthalpy change (ΔH), entropy change (ΔS) and Gibbs free energy change (ΔG) could be determined. From the enthalpy change, endothermic and exothermic nature of the system could be determined; the degree of disorderliness of the system would be determined from the change in entropy while Gibbs free energy change gives information about the feasibility and spontaneity of the system. Figure 22 below shows the effect of temperature on the adsorption of Cu²⁺ onto nZVMn. Five different temperatures (298, 308, 318, 328 and 338 K) were investigated in this research. It can be inferred that increase in temperature led to increase in the removal efficiency of Cu²⁺ which may be due to increase in number of active sites and the decrease in the thickness of the boundary layer surrounding the adsorbent with temperature, so that the mass transfer resistance of adsorbate in the boundary layer decreases (Dogan et al. 2009). Moreover, increasing temperature resulted in an increase in the rate of approach to equilibrium. The positive value of enthalpy change indicated that the adsorption process of Cu(II) ions onto nZVMn was endothermic. This was further confirmed by the Van't Hoff plot.

Table 5 Comparison of the adsorption capacities of nano-adsorbent used for Cu^{2+} removal

S/N	Adsorbents	Adsorption capacity (Q_{\max}) (mg/g)	References
1	Magnetite	126.9	Febrianto et al. (2009)
2	Kaolin Fe/Ni nanoparticles	107.8	Xiao et al. (2011)
3	S-doped TiO_2	96.3	Li et al. (2011)
4	Magnetic nanoparticles coated by chitosan carrying of [1]-ketoglutaric acid	96.15	Zhou et al. (2009)
5	Pectin-iron oxide	48.99	Gong et al. (2012)
6	Carboxymethyl- β -cyclodextrin-conjugated magnetics nanoparticle	47.29	Badruddoza et al. (2011)
7	Fe_3O_4 magnetic nanoparticles coated with humic acid	46.3	Liu et al. (2013)
8	Magnetic gamma- Fe_2O_3 nanoparticles coated with poly-L-cysteine	42.9	White et al. (2009)
9	Magnetic nano-adsorbent modified by gum arabic	38.5	Banerjee and Chen (2007)
10	Hydroxyapatite nanoparticles	36.9	Wang et al. (2009)
11	Maghemite nanoparticle	27.7	Hu et al. (2006)
12	Amino-functionalized magnetic nanosorbent	25.77	Hao et al. (2010)
13	Chitosan-bound Fe_3O_4 magnetic nanoparticles	21.5	Chang and Chen (2005)
14	Manganese nanoparticles	181.82	This present study

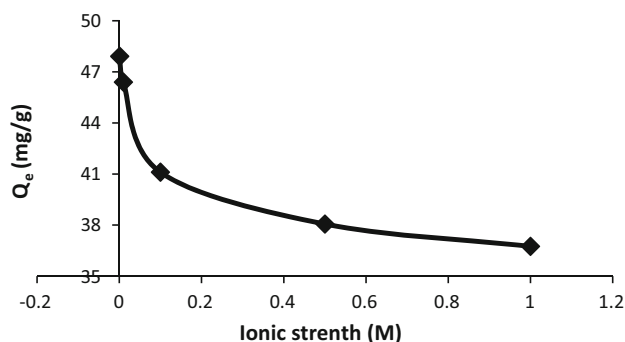
**Fig. 22** Effect of temperature on Cu^{2+} adsorbed onto nZVMn. Experimental conditions: optimum Cu^{2+} concentration = 100 ppm; volume of Cu^{2+} solution = 50 mL; nZVMn dose = 100 mg; pH = 5, contact time = 60 min, and temperature = 25 ± 2 °C**Fig. 23** Van't Hoff plot on sorption of Cu^{2+} onto nZVMn nano-adsorbent

The Van't Hoff plot of $\log K_c$ versus $1/T$ in Fig. 23 gave a straight line and the thermodynamic parameters, standard enthalpy change ΔH° (kJ mol^{-1}) and standard entropy

Table 6 Thermodynamic parameters for adsorption of Cu^{2+} onto nZVMn

T (°C)	T (K)	ΔG (kJ mol^{-1})	ΔH (kJ mol^{-1})	ΔS ($\text{J mol}^{-1} \text{K}^{-1}$)	Ka
25	298	-9.29891	+50.27848	+203.5724	42.63002
35	308	-13.3685			184.8736
45	318	-15.1904			312.4796
55	328	-16.9041			491.6108
65	338	-17.4473			496.5124

change ΔS° ($\text{J mol}^{-1} \text{K}^{-1}$) were determined from the slope and intercept, respectively. The standard Gibbs free energy ΔG° (kJ mol^{-1}), was calculated using the Eq. 30. Table 6 below shows the values of thermodynamic parameters of the adsorption of Cu^{2+} onto nZVMn. It can, therefore, be ascertained from the positive value of ΔH ($\Delta H = + 50.27848$

**Fig. 24** Ionic strength on Cu^{2+} adsorbed onto nZVMn. Experimental conditions: Cu^{2+} concentration = 100 ppm; volume of Cu^{2+} solution = 50 mL; nZVMn dose = 100 mg; pH = 5, contact time = 60 min, stirring speed = 200 rpm and temperature = 25 ± 2 °C

kJ mol^{-1}) that the reaction is endothermic (Table 6). The standard entropy change ΔS° ($203.5724 \text{ J mol}^{-1} \text{ K}^{-1}$) indicated the degree of randomness at the solid–liquid interface during the adsorption of Cu^{2+} onto nZVMn and the negative values of the standard Gibbs free energy ΔG° indicated the feasibility and spontaneity of the adsorption process. This finding is in support with the report of other researchers (Hao et al. 2010; Lisha et al. 2010).

Effect of salinity on adsorption of Cu(II)

Figure 24 shows the influence of salinity (ionic strength) on Cu^{2+} adsorbed onto nZVMn at optimum conditions. This investigation was carried out using NaCl solution of different ionic strength from 0.001 to 1.0 M. Increase in ionic strength led to decrease in the percentage removal efficiency from 95.82 to 73.49 % and the quantity adsorbed also decreased from 47.91 to 36.75 mg/g. This decrease in the amount of copper uptake was due to increase in the electrostatic attraction arising from compressed electrical diffuse double layer. Also, increase in the number of adsorbate species led to electrostatic competition between copper ions and sodium ions on the available adsorption sites (Liu et al. 2013; Gong et al. 2012; Xiao et al. 2011; Hao et al. 2010; Dogan et al. 2009; Larous et al. 2005).

Conclusion

This study has successfully investigated the synthesis, characterization and application of novel zerovalent manganese nanoparticle for adsorption of Cu^{2+} . Results from this study suggested that adsorption of Cu^{2+} depended on all operational factors such as effect of initial concentration, contact time, pH, adsorbent dose, agitation speed, and temperature investigated. Pseudo second order well described the kinetics of the process and the mechanism was governed by pore diffusion which was validated by sum of square error (SSE), Chi-square (χ^2) and normalized standard variation (Δq) % statistical models. The equilibrium data fitted well to Langmuir, Freundlich, Temkin, DKR and Halsey isotherm models. However, the value of the mean energy evaluated from DKR model indicated that electrostatic force played a role in adsorption process. The thermodynamic studies showed that the adsorption process is feasible, endothermic and spontaneous in nature. Outcome of this study enlisted nanoscale zerovalent manganese (nZVMn) as a potential and novel nano-adsorbent for the adsorption of heavy metal ions and can be recommended for industrial treatment of effluent.

Acknowledgments Dada, Adewumi Oluwasogo appreciates the Management of Landmark University for giving me the opportunity to

undertake and finish my Ph.D. programme in University of Ilorin. The assistance rendered by Ogunlaja Adeniyi in Rhodes University, South Africa for the TEM, SEM and EDX analyses is highly appreciated.

Open Access This article is distributed under the terms of the Creative Commons Attribution 4.0 International License (<http://creativecommons.org/licenses/by/4.0/>), which permits unrestricted use, distribution, and reproduction in any medium, provided you give appropriate credit to the original author(s) and the source, provide a link to the Creative Commons license, and indicate if changes were made.

References

- Adekola FA, Abdus-Salam N, Adegoke HI, Adesola MA, Adekeye JID (2012) Removal of Pb(II) from aqueous solution by natural and synthetic calcites. *Bull Chem Soc Ethiop* 26(2):195–210
- Ahmad MA, Ahmad N, Bello OS (2014a) Adsorptive removal of malachite green dye using durian seed-based activated carbon. *Water Air Soil Pollut* 225:2057. doi:10.1007/s11270-014-2057-z
- Ahmad MA, Ahmad N, Bello OS (2014) Modified durian seed as adsorbent for the removal of methyl red dye from aqueous solutions. *Appl Water Sci*. doi:10.1007/s13201-014-0208-4
- Ahmad MA, Puad NAA, Bello OS (2014c) Kinetic, equilibrium and thermodynamic studies of synthetic dye removal using pomegranate peel activated carbon prepared by microwave-induced KOH activation. *Water Res Ind*. doi:10.1016/j.wri.2014.06.002
- Ayanda OS, Fatoki SO, Adekola FA, Ximba BJ (2013) Kinetics and equilibrium models of the adsorption of tributyltin to nZnO, activated carbon and nZnO/activated carbon composite in artificial seawater. *Mar Pollut Bull*. doi:10.1016/j.marpolbul.2013.04.001
- Badruddoza AZM, Tay ASH, Tan PY, Hidajat K, Uddin MS (2011) Carboxymethyl- β -cyclodextrin conjugated magnetic nanoparticles as nano-adsorbents for removal of copper ions: synthesis and adsorption studies. *J Hazard Mater* 185:1177–1186
- Banerjee SS, Chen DH (2007) Fast removal of copper ions by gum arabic modified magnetic nano-adsorbent. *J Hazard Mater* 147:792–799
- Basar CA (2006) Applicability of the various adsorption models of three dyes adsorption onto Activated Carbon Prepared from Waste Apricot. *J Hazard Mater B* 135:232–241
- Bello OS, Ahmad MA, Semire B (2014) Scavenging malachite green dye from aqueous solutions using pomelo (*Citrus grandis*) peels: kinetic, equilibrium and thermodynamic studies. *Desalin Water Treat*. doi:10.1080/19443994.2014.940387
- Bhatt RR, Shah BA (2013) Adsorption studies of heavy metal ions by salicylic acid–formaldehyde–catechol terpolymeric resin: isotherm, kinetic and thermodynamics. *Arabian J Chem*. doi:10.1016/j.arabjc.2013.03.012(2013)
- Bonnie RS, Marc S, Daniel K, Peter A, Tar-Ching SB et al (2007) Copper and human health: biochemistry, genetics, and strategies for modeling dose-response relationships. *J Toxicol Environ Health Part B* 10:157–222
- Boparai HK, Meera J, Dennis MO (2010) Kinetics and thermodynamics of cadmium ion removal by adsorption onto nano zerovalent iron particles. *J Hazard Mater*. doi:10.1016/j.jhazmat.2010.11.029
- Brewer GJ (2010) Copper toxicity in the general population. *Clin Neurophysiol* 121(4):459–460. doi:10.1016/j.clinph.209.12.015PMID20071223
- Cai X, Gao Y, Sun Q, Chen Z, Megharaj M, Naidu R (2014) Removal of co-contaminants Cu(II) and nitrate from aqueous solution using kaolin-Fe/Ni nanoparticles. *Chem Eng J* 244:19–26

- Chang YC, Chen DH (2005) Preparation and adsorption properties of monodisperse chitosan-bound Fe_3O_4 magnetic nanoparticles for removal of $\text{Cu}(\text{II})$ ions. *J Colloid Interface Sci* 283:446–451
- Chen Z-X, Jin X-Y, Chen Z, Megharaj M, Naidu R (2011) Removal of methyl orange from aqueous solution using bentonite-supported nanoscale zero-valent iron. *J Colloid Interface Sci* 363:601–607
- Chingombe P, Saha B, Wakeman RJ (2006) Adsorption of atrazine on conventional and surface modified activated carbons. *J Colloid Interface Sci* 302:408–416
- Cho D-W, Jeon B-H, Chon C-M, Kim Y, Schwartz FW, Lee E-S, Song H (2012) A novel chitosan/clay/magnetite composite for adsorption of $\text{Cu}(\text{II})$ and $\text{As}(\text{V})$. *Chem Engg J* 200–202:654–662
- Dada AO, Adekola FA, Odeunmi EO (2014) Investigation of the synthesis and characterization of manganese nanoparticles and its ash rice husk supported nanocomposite. In: Book of proceedings of 1st African International Conference/Workshop on applications of nanotechnology to energy, health and environment—March 23rd–29th
- Dada AO, Adekola FA, Odeunmi EO (2014) Kinetics, isotherms and thermodynamics studies of adsorption of Cu^{2+} onto novel zerovalent iron nanoparticles. *Covenant J Phys Life Sci* 2(1):24–53
- Doğan M, Türkyılmaz A, Alkan M, Demirbaş Ö (2009) Adsorption of copper (II) ions onto sepiolite and electrokinetic properties. *Desalination* 238:257–270
- Edison TJI, Sethuraman MG (2013) Biogenic robust synthesis of silver nanoparticles using Punica granatum peel and its application as a green catalyst for the reduction of an anthropogenic pollutant 4-nitrophenol. *Spectrochim Acta Part A Mol Biomol Spectrosc* 104:262–264
- Febrianto J, Kosasih AN, Sunarso J, Ju Y-H, Indraswati N, Ismadji S (2009) Equilibrium and kinetic studies in adsorption of heavy metals using biosorbent: a summary of recent studies. *J Hazard Mater* 162:616–645
- Foo KY, Hameed BH (2010) Review: insights into the modeling of adsorption isotherm systems. *Chem Engg J* 156:2–10
- Gong J, Chen L, Zeng G, Long F, Deng J, Niu Q, He X (2012) Shellac-coated iron oxide nanoparticles for removal of cadmium (II) ions from aqueous solution. *J Environ Sci* 24(7):1165–1173
- Gonga J-L, Wanga X-Y, Zeng G-M, Chen L, Denga J-H, Zhang X-R, Niu Q-Y (2012) Copper (II) removal by pectin-iron oxide magnetic nanocomposite adsorbent. *Chem Engg J* 185–186:100–107
- Hameed BH, Mahmoud DK, Ahmad AL (2008) Equilibrium modeling and kinetic studies on the adsorption of basic dye by a low-cost adsorbent: coconut (*Cocos nucifera*) bunch waste. *J Hazard Mater* 158:65–72
- Hao Y-M, Chen M, Hu Z-B (2010) Effective removal of $\text{Cu}(\text{II})$ ions from aqueous solution by amino-functionalized magnetic nanoparticles. *J Hazard Mater* 184:392–399
- Harkins WD, Jura GJ (1944) The decrease of free surface energy as a basis for the development of equations for adsorption isotherms; and the existence of two condensed phases in films on solids. *J Chem Phys* 12:112–113
- Ho YS (2004) Pseudo-isotherms using a second order kinetic expression constant. *Adsorption* 10:151–158
- Ho YS, McKay G (2003) Adsorption of dyes and copper ions onto bio-sorbents. *Process Biochem* 38:1047–1061
- Hu J, Chen GH, Lo IMC (2006) Selective removal of heavy metals from industrial wastewater using maghemite nanoparticle: Performance and mechanisms. *J Environ Eng ASCE* 132:709–715
- Huang S-H, Chen D-H (2009) Rapid removal of heavy metal cations and anions from aqueous solutions by an amino-functionalized magnetic nano-adsorbent. *J Hazard Mater* 163:174–179
- Igwe JC, Abia AA (2006) A bioseparation process for removing heavy metals from waste water using biosorbents. *African J Biotechnol* 5(12):1167–1179
- Igwe JC, Abia AA, Ibeh CA (2005) Adsorption kinetics and intraparticle diffusivities of Hg, As and Pb ions on unmodified and thiolated coconut fiber. *Int J Environ Sci Technol* 5:83–92
- Jaafar MZ, Nasir AM, Hamid MF (2013) Point of zero charge for sandstone and carbonate rocks by streaming potential. *Int J Pet Geosci Eng* 1(2):82–90
- Jain PL, Huang X, El Sayed LH, El Sayed MA (2007) Review of some interesting surface plasmon resonance-enhanced properties of noble metal Nanoparticles and their applications to biosystems. *Plasmonics* 2:107–118
- Kara A, Demirbel E (2012) Physicochemical parameters of $\text{Cu}(\text{II})$ ions adsorption from aqueous Solution by magnetic-poly(divinylbenzene-*N*-vinylimidazole) microbeads. *Sep Sci Technol* 47(5):709–722
- Karabellia D, Ünal S, Shahwan T, Eröglu AE (2011) Preparation and characterization of alumina-supported iron nanoparticles and its application for the removal of aqueous Cu^{2+} ions. *Chem Eng J* 168:979–984
- Kumar V, Yadav KS (2011) Synthesis of stable, polyshaped silver, and gold nanoparticles using leaf extract of *Lonicera japonica* L. *Int J Green Nanotechnol* 3:281–291
- Kumar PS, Vincent C, Kirthika K, Kumar KS (2010) Kinetics and equilibrium studies of Pb^{2+} ion removal from aqueous solutions by use of nano-silversolcoated activated carbon. *Braz J Chem Eng* 27:339–346
- Larous S, Meniai AH, Lehocine BM (2005) Experimental study of the removal of copper from aqueous solution by adsorption using Sawdust. *Desalination* 185:483–490
- Li E, Zeng X, Fan Y (2009) Removal of chromium ion (III) from aqueous solution by manganese oxide and microemulsion modified diatomite. *Desalination* 238:158–165
- Li D, Wang X, Wan D, Duan S, Liu C, Zhang K, Fang B (2011) Adsorption of Cu^{2+} cations from aqueous solution by S-doped TiO_2 . *Sep Sci Technol* 46:2539–2548
- Lisha KP, Shihabudheen M, Pradeep MT (2010) Manganese dioxide nanowhiskers: a potential adsorbent for the removal of $\text{Hg}(\text{II})$ from water. *Chem Eng J* 160:432–439
- Liu JF, Zhao ZS, Jiang GB (2008) Coating Fe_3O_4 magnetic nanoparticles with humic acid for high efficient removal of heavy metals in water. *Environ Sci Technol* 42:6949–6954
- Liu W, Wang T, Borthwick AGL, Wang Y, Yin X, Li X, Ni J (2013) Adsorption of Pb^{2+} , Cd^{2+} , Cu^{2+} and Cr^{3+} onto titanate nanotubes: competition and effect of inorganic ions. *Sci Total Environ* 456–457:171–180
- Prasad TNVKV, Elumalai EK (2011) Biofabrication of Ag nanoparticles using moringa oleifera leaf extract and their antimicrobial activity. *Asian Pac J Trop Biomed* 1(6):439–442. doi:10.1016/S2221-1691(11)60096-8
- Prathna TC, Mathew L, Chandrasekaran N, Raichur AM, Mukherjee A (2012) Biomimetic synthesis of nanoparticles: science, technology and applicability, School of BioSciences and Technology, VIT University Department of Materials Engg., Indian Institute of Science, India, pp 1–20
- Ren YM, Wei XZ, Zhang ML (2008) Adsorption character for removal $\text{Cu}(\text{II})$ by magnetic $\text{Cu}(\text{II})$ ion imprinted composite adsorbent. *J Hazard Mater* 158:14–22
- Roosta M, Ghaedi M, Daneshfar A, Sahraei R, Asghari A (2014) Optimization of the ultrasonic assisted removal of methylene blue by gold nanoparticles loaded on activated carbon using experimental design methodology. *Ultrason Sonochemistry* 21(1):242–252
- Sikdera T, Mihara Y, Islam S, Saito T, Tanaka S, Kurasaki M (2014) Preparation and characterization of chitosan-caboxymethyl- β -

- cyclodextrin entrapped nanozerovalent iron composite for Cu(II) and Cr(IV) removal from wastewater. *Chem Engg J* 236:378–387
- Sinha A, SinghVN Mehta BR, Khare SK (2011) Synthesis and characterization of monodispersed orthorhombic manganese oxide nanoparticles produced by *Bacillus* sp. cells simultaneous to its bioremediation. *J Hazard Mater* 192:620–627
- Song C, Wu S, Cheng M, Tao P, Shao M, Gao G (2014) Adsorption studies of coconut shell carbons prepared by KOH activation for removal of lead (II) from aqueous solutions. *Sustainability* 6:86–98. doi:[10.3390/su6010086](https://doi.org/10.3390/su6010086)
- Srivastava VC, Mall ID, Mishra IM (2005) Characterization of mesoporous rice husk ash (RHA) and adsorption kinetics of metal ions from aqueous solution onto RHA. *J Hazard Mater*. doi:[10.1016/j.jhazmat.11.052](https://doi.org/10.1016/j.jhazmat.11.052)
- Temkin MI, Pyzhev V (1940) Kinetic of ammonia synthesis on promoted iron catalysts. *Acta Physiochim URSS* 12:327–356
- Waghmare SS, Deshmukh AM, Kulkarni SW, Oswaldo LA (2011) Biosynthesis and characterization of manganese and zinc nanoparticles. *Univers J Environ Res Technol* 1:64–69
- Wang YJ, Chen JH, Cui YX, Wang SQ, Zhou DM (2009) Effects of low-molecular weight organic acids on Cu(II) adsorption onto hydroxyapatite nanoparticles. *J Hazard Mater* 162:1135–1140
- Weber WJ, Morris JC (1963) Kinetics of adsorption on carbon from solution. *J Sanit Eng Div ASCE* 89:31–59 (**Mater** 161:848–853)
- White BR, Stackhouse BT, Holcombe JA (2009) Magnetic gamma-Fe₂O₃ nanoparticles coated with poly-L-cysteine for chelation of As(III), Cu(II), Cd(II), Ni(II), Pb(II) and Zn(II). *J. Hazard. Mater.* 161:848–853
- Wojtysiak W, Kudelski A (2012) Influence of oxygen on the process of formation of silver nanoparticles during citrate/borohydride synthesis of silver sols. *Colloids Surf A Physicochem Engl Asp* 410:45–51
- Wu FC, Tseng RI, Jung RS (2001) Kinetic modeling of liquid-phase adsorption of reactive dyes and metal ions on chitosan. *Water Res* 35:613–618
- Xi Y, Megharaj M, Naiduv R (2011) Dispersion of zerovalent iron nanoparticles onto bentonites and use of these catalysts for orange II decolourisation. *Appl Clay Sci* 53:716–722
- Xiao S, Ma H, Shen M, Wang S, Huang Q, Shi X (2011) Excellent copper (II) removal using zero-valent iron nanoparticle-immobilized hybrid electrospun polymer nanofibrous mats. *Colloids Surf A Physicochem Engl Asp* 381:48–54
- Xu H, Liu Y, Tay J (2006) Effect of pH on nickel bioadsorption by aerobic granular sludge''. *Bioresour Technol* 97(3):359–363
- Zhou YT, Nie HL, Branford-White C, He ZY, Zhu LM (2009) Removal of Cu²⁺ from aqueous solution by chitosan-coated magnetic nanoparticles modified with α -ketoglutaric acid. *J Colloid Interface Sci* 330:29–37